Eur. Phys. J. Plus (2022) 137:1316
https://doi.org/10.1140/epjp/s13360-022-03504-x

THE EUROPEAN PHYSICAL JOURNAL PLUS

Regular Article

Signatures of excited monopolium

Huner Fanchiotti[1], **Carlos A. García Canal**[1], **Marco Traini**[2], **Vicente Vento**[3,a]

[1] IFLP(CONICET) and Department of Physics, University of La Plata, C.C. 67 1900 La Plata, Argentina
[2] Dipartimento di Fisica, Università degli Studi di Trento, Via Sommarive 14, Povo, 38123 Trento, Italy
[3] Departamento de Física Teórica and IFIC, Universidad de Valencia, CSIC, Burjassot, 46100 Valencia, Spain

Received: 29 September 2022 / Accepted: 16 November 2022

Abstract We study electromagnetic properties of particles with magnetic moment and no charge using their behavior when traversing coils and solenoids. These particles via the Faraday-Lenz law create a current whose energy we calculate. We analyze both the case of very long lived, almost stable, particles and those with a finite lifetime. We use this development to study the behavior of monopolium a monopole-antimonopole bound state in its excited states.

1 Introduction

Monopoles and their detection have been a matter of much research since Dirac discovered his now famous quantization condition [1, 2],

$$eg = \frac{N}{2} \quad N = 1, 2, \ldots, \tag{1}$$

where e is the electron charge, g is the monopole magnetic charge and we have used natural units $\hbar = c = 4\pi\varepsilon_0 = 1$.

In Dirac's formulation, monopoles are assumed to exist as point-like particles and quantum mechanical consistency conditions lead to establish the magnitude of their magnetic charge. Monopole physics took a dramatic turn when 't Hooft [3] and Polyakov [4] independently discovered that the SO(3) Georgi–Glashow model [5] inevitably contains monopole solutions. These topological monopoles are impossible to create in particle collisions because of their huge GUT scale mass [6] or in other models with lower mass because of their complicated multi-particle structure [7].

In Dirac's formulation, since the magnetic charge is conserved, monopoles should be produced predominantly in monopole-antimonopole pairs. Inspired by the old idea of Dirac [1] and Zeldovich [8] that monopoles are not seen free because they are confined by their strong magnetic forces, we have studied a monopole-antimonopole bound state that we have called monopolium [9]. This state is the strongly coupled dual analog of positronium and decays into photons [10].

The discovery of monopole and dipole solutions in Kaluza–Klein theories [11, 12] made these theories very exciting from a theoretical point of view [13]. In particular, the dipole solution, which is classically stable and therefore very long lived, forms a very interesting state which we have also called monopolium in analogy with its decaying cousin in gauge theories. The Kaluza–Klein monopolium is extremely massive with a mass of the order of the Planck mass and therefore impossible to produce in laboratories. However, there might be clouds of them in the cosmos which might enter our detectors [14].

Much experimental research has been carried out into the search for monopoles [15–19]. However, our interest here lies in the detection of monopolium, who is chargeless but which can manifest a magnetic moment in the presence of magnetic fields or in excited deformed states [14, 20]. Our aim here is to study the behavior of monopolium in the presence of coils and solenoids to determine interesting properties and energy regimes of excited monopolia which may serve as a guide to more sophisticated experiments given the progress of electromagnetic technologies at present.

In what follows, we are going to discuss methods to study magnetic moments and how they might be used in the study of particle properties. In Sect. 2, we describe the effects of a particle with a magnetic dipole moment when traversing conducting coils. In Sect. 3, we determine the observables characterizing particles with magnetic moment and no electromagnetic charges. In Sect. 4, we describe the behavior of monopolium when traversing coils and solenoids. In Sect. 5, we apply the unveiled properties of monopolium to describe possible signatures of cosmic monopolium. We end in Sect. 6 by collecting the most significant results of our investigation.

[a] e-mail: vicente.vento@uv.es (corresponding author)

Published online: 07 December 2022

2 Effects of a particle with magnetic dipole moment passing through a conducting coil

Our subject of study is a particle which has a permanent or an induced magnetic dipole moment $\overrightarrow{\mathcal{M}}$. We call this particle dipole for short. Assuming the size of the particle small compared with the distance at which we are measuring the magnetic field, its dipole moment will produce a magnetic field [20]

$$\overrightarrow{B}_d(\vec{r}) = \frac{3(\overrightarrow{\mathcal{M}} \cdot \vec{r})\,\vec{r} - \overrightarrow{\mathcal{M}}\, r^2}{r^5}, \tag{2}$$

where $r = |\vec{r}| = \sqrt{(x-x_0)^2 + (y-y_0)^2 + (z-z_0)^2}$, (x, y, z) is any point in space and (x_0, y_0, z_0) is the position of the dipole considered point-like for this calculation.

Let the dipole travel with a constant velocity toward a circular conducting coil of radius R with its magnetic moment perpendicular to the plane of the coil as shown in Fig. 1. Let S' be the reference system associated to the dipole and S is the reference system associated to the coil. We choose the coil to be located in the $z = 0$ plane, thus at time t, the dipole will be located at $z = -vt$. The magnetic field felt by any point of space $\vec{r'} = (x', y', z')$ when the dipole is $\overrightarrow{\mathcal{M}} = \mathcal{M}\,\hat{k'}$ is

$$\overrightarrow{B'}_d(\vec{r'}) = \frac{3\mathcal{M}(\hat{k'} \cdot \vec{r'})\,\vec{r'} - \mathcal{M}\,\hat{k'}\, r'^2}{r'^5}, \tag{3}$$

where $r' = |\vec{r'}| = \sqrt{x'^2 + y'^2 + z'^2}$ and $\hat{k'}$ is the unit vector in the z direction. We need the magnetic field at the coil. The Lorentz transformation from reference system S' to the reference system S is given by

$$\begin{aligned} x' &= x, \\ y' &= y, \\ z' &= \gamma(z - vt), \\ t' &= \gamma(t - z), \end{aligned}$$

where $\gamma = 1/\sqrt{1 - v^2}$. Since we have no electric field present, the magnetic field changes [21]

$$B'_x = \gamma B_x, \tag{4}$$

$$B'_y = \gamma B_y, \tag{5}$$

$$B'_z = B_z. \tag{6}$$

With this geometry, the flux through the coil is

$$\Phi(t) = \int_0^R d\rho \int_0^{2\pi} \mathrm{d}\varphi\ \overrightarrow{B}_d(x, y, -\gamma vt) \cdot \hat{k}, \tag{7}$$

where ρ and φ are the polar coordinates in the $z = 0$ plane of the coil and R is the radius of the coil. This calculation can be performed analytically and leads to

$$\Phi(t) = -\frac{2\mathcal{M}\pi R^2}{((\gamma vt)^2 + R^2)^{3/2}}. \tag{8}$$

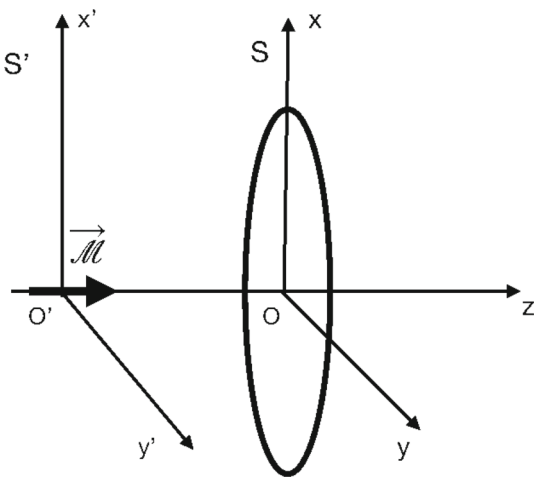

Fig. 1 Our set up: a particle traveling with constant velocity toward a conducting coil with its magnetic dipole moment perpendicular to the plane of the coil. S' is the reference system associated to the dipole and S is the one associated to the coil

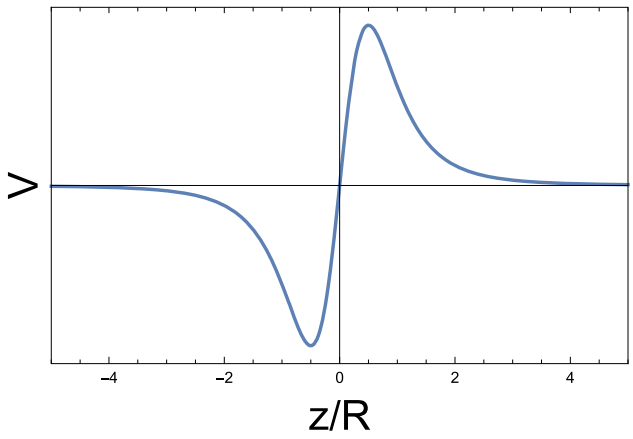

Fig. 2 Functional form of the voltage generated by a dipole with a magnetic moment passing a conducting coil at uniform speed

Applying the Faraday–Lenz law, the induced electromotive force (EMF) generated by the magnetic field becomes

$$V(\gamma\, v\, t, R) = \frac{6\mathcal{M}\pi R^2(\gamma v)^2 t}{((\gamma v t)^2 + R^2)^{5/2}}. \tag{9}$$

This equation can be written using $z(t) = \gamma v t$, the area of the coil $A = \pi R^2$ and the strength parameter $\chi = 6\mathcal{M}\gamma v$ as

$$V(z, A, \chi) = \frac{\chi A z}{(z^2 + \frac{A}{\pi})^{5/2}}. \tag{10}$$

This function is presented in Fig. 2 for fixed A and χ.

We have assumed in the previous calculation that the dipole passes through the axis of the coil. Reference [21] shows the result when the dipole does not pass through the axis, which is non analytic. Off axis, the shape of the pulse is asymmetric and the time span shorter. For the purposes of the estimates which will be calculated in this presentation, Eq. (10) will be sufficient, with the advantage of being analytic.

A simple mathematical calculation determines the position of the extrema at

$$z = \pm\frac{1}{2}\sqrt{\frac{A}{\pi}} = \pm\frac{1}{2}R, \tag{11}$$

where the voltage takes the value

$$V\left(\pm\frac{1}{2}\sqrt{\frac{A}{\pi}}, A, \chi\right) = \pm\frac{16\pi^2\chi}{25\sqrt{5}A}. \tag{12}$$

The signal, a rise in the voltage, is governed by two parameters the strength χ and the area of the coil, being proportional to the former and inversely proportional to the latter, thus the ideal radius of the coil R has to be as small as possible compatible with all the approximations.

Let us introduce a system with a large number of coils close to each other forming a cylinder. There are two ways of creating this solenoid, either with well separated coils or with closely winded coils. In the first case, as shown in Fig. 3, the effect is simply to add the effect of each coil almost independently.

If the coils are very close, the effect is more sophisticated; the advantage being that we can put many coils in a shorter length to produce an enhancement of the coil effect in shorter distance. This case requires a detailed calculation that can be performed numerically:

$$V_N(z, A, \chi, L) = \sum_{n=1}^{n=N} V(z - (n-1)\Delta z, A, \chi), \tag{13}$$

where V is the potential in Eq. (10), N is the number of coils, L is the length of the coil cylinder and $\Delta z = \frac{L}{N}$. We show in Fig. 4 V/N generated by 50, 500 and 5000 coils located between $0 \leq \frac{z}{R} \leq 5$. This result is only valid for a large number of coils, when there is a cancelation between the positive and negative potentials.

Doing some numerical analysis, we find the relation between the maxima of the single coil potential and the N coil potential for N large

$$\frac{V_N(\max)}{N} \sim 0.1312\sqrt{A}\, V_1(\max) \sim 0.3706\frac{\chi}{\sqrt{A}}. \tag{14}$$

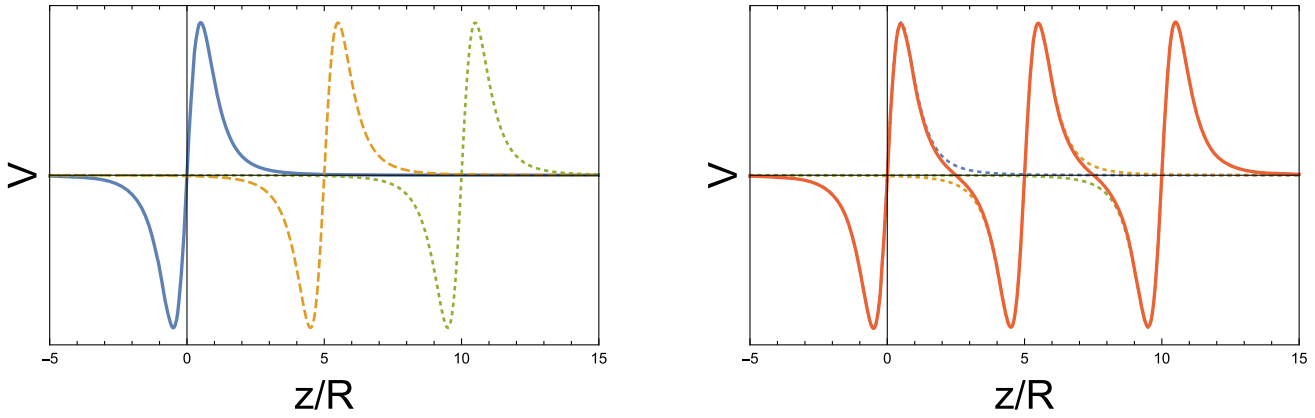

Fig. 3 The left figure shows the functional form of the voltage generated by a particle with a magnetic moment when passing three independent coils at uniform speed. The figure on the right shows the combined effect of the three well separated coils forming a solenoid (solid curve) compared with the independent effect of the three coils (dotted curve). The effect is basically the same effect as that of the three coils independently

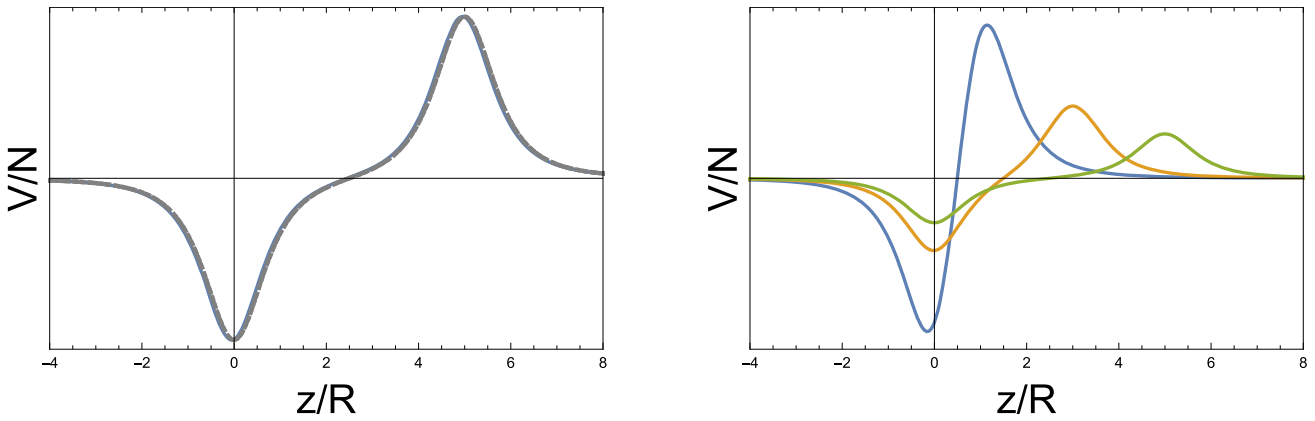

Fig. 4 The left figure shows the functional form of the voltage generated by a particle with a magnetic moment when passing a system of conducting coils of length $5R$ at uniform speed. The distance between the peaks is the length of the system of coils. The figure is composed by the calculation of the voltage for 50, 500 and 5000 loops divided by the number of loops showing that the proportionality between number of loops and voltage persists for relatively large lengths of the systems of coils. The figure on the right shows the same for three different lengths of the coils' system. The shorter the length, the greater the voltage

Moreover, we are able to find an approximate analytical solution valid for large N

$$\begin{aligned} \frac{V^{\text{in}}_{N\,\text{approx}}(z)}{N} &\sim \frac{-b}{\left(z^2+\frac{a}{\pi}\right)^{5/2}}, \\ \frac{V^{\text{out}}_{N\,\text{approx}}(z)}{N} &\sim \frac{b}{\left((z-L)^2+\frac{a}{\pi}\right)^{5/2}}, \end{aligned} \tag{15}$$

where $a = 2A$ and $b = 0.1198\,\chi\,A^2$. The *in* potential describes the approximation to the incoming minimum and the *out* potential the approximation to the outcoming maximum. In Fig. 5, we show the result of the exact calculation for $N = 1000$ and compare it to the approximation for the mentioned values of the parameters.

It is interesting to note from the above expression that the peak of the potential depends directly on the magnitude of the magnetic dipole moment and is inversely proportional to the square root of the area of the coil. This means that one does not need large coil sizes to reveal the magnetic dipole moment. Certainly, there are limitations to the sizes due to the approximations used, i.e., for circular coils $A = \pi R^2$ and R has to be much bigger than the section of the coil. The result of the calculation shows that the voltage scales nicely with the number of coils and that the smaller the coil system, the higher the potential for the same number of coils. One has thus to find a compromise between length and number of coils. The width of the coil has not been taken into account in this calculation, but its effect is irrelevant at this point as long as its size s is smaller than R.

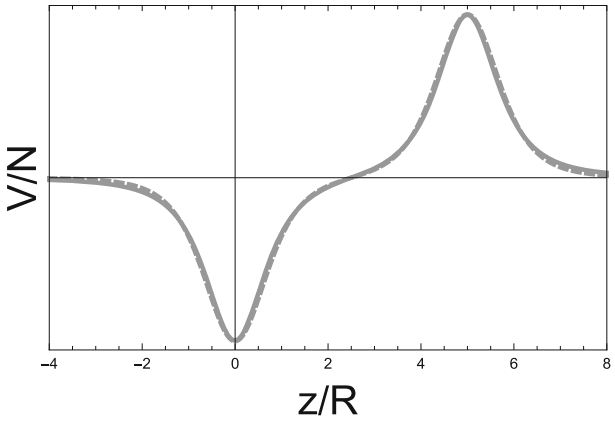

Fig. 5 Functional form of the exact numerical calculation Eq. (13) (solid) and the approximate one Eq. (15) (dashed) for $N = 1000$, $L = 5R$ $A = 0.1R^2$ and $\chi = 0.5\ \mathrm{V}\cdot R$

3 Determination of observables characterizing particles with magnetic moment and no electromagnetic charges

In the first subsection, we will calculate the current created in systems of coils by the moving dipole as a means of characterizing particles with magnetic moment and no charge. In the second subsection, we will study the same effects on particles with magnetic moments of finite lifetime. In the third subsection, we study the effect on the particle motion of this induced current which turns out to be small.

3.1 The induced current and the deposited energy in coil systems

A dipole traversing a single coil creates a magnetic field due to the $\overrightarrow{\mathcal{M}}\cdot\hat{k}$ component of its magnetic dipole moment whose flux in the coil generates, via the Faraday-Lenz law, an EMF Eq. (9),

$$V_1(z) = 6\mathcal{M}_z\,\gamma\,v\,A\,z\frac{1}{\left(z^2+\frac{A}{\pi}\right)^{5/2}}. \tag{16}$$

Only the z component of the magnetic moment $\overrightarrow{\mathcal{M}}\cdot\hat{k} = \mathcal{M}_z = \mathcal{M}\cos\theta$, where $\cos\theta = \frac{\overrightarrow{\mathcal{M}}\cdot\hat{k}}{\mathcal{M}}$ is active. Since we expect the dipoles initially in random directions in the forward direction, the average $\mathcal{M}_z$ will be M multiplied by the factor,

$$\frac{\int_0^{2\pi}\mathrm{d}\varphi\int_{-\frac{\pi}{2}}^{+\frac{\pi}{2}}\mathrm{d}\theta\cos\theta}{\int_0^{2\pi}\mathrm{d}\varphi\int_{-\frac{\pi}{2}}^{+\frac{\pi}{2}}\mathrm{d}\theta} = \frac{2}{\pi}. \tag{17}$$

and therefore, Eq. (16) becomes

$$V_1(z) = \frac{12}{\pi}\mathcal{M}\,\gamma\,v\,A\,z\frac{1}{\left(z^2+\frac{A}{\pi}\right)^{5/2}}. \tag{18}$$

For the N coil solenoid, recalling Eq. (15), the EMF becomes

$$\begin{aligned} V_N^{\mathrm{in}}(z) &\sim -0.4576\,\mathcal{M}\,\gamma\,v\,N\,A^2\frac{1}{\left(z^2+\frac{2A}{\pi}\right)^{5/2}},\\ V_N^{\mathrm{out}}(z) &\sim +0.4576\,\mathcal{M}\,\gamma\,v\,N\,A^2\frac{1}{\left((z-L)^2+\frac{2A}{\pi}\right)^{5/2}}, \end{aligned} \tag{19}$$

where N is the number of coils in each coil system and L is its length.

The total EMF has to take into account the inductance, thus

$$V_T = -\frac{d\Phi}{dt} - \mathfrak{L}\frac{d\mathcal{I}}{dt}, \tag{20}$$

where $\mathfrak{L}$ is the inductance and $\mathcal{I}$ is the intensity of the current in the circuit. Ohm's law then becomes the differential equation we have to solve in order to obtain the intensity in the circuit

$$\frac{d\Phi}{dt} + \mathfrak{L}\frac{d\mathcal{I}}{dt} + \mathcal{I}\mathcal{R} = 0. \tag{21}$$

where $\mathcal{R} = \frac{2\pi R}{S}\varrho N$, where S is the section of the conductor and ϱ is the resistivity which changes from conventional conductors, $\varrho = 10^{-8}$ Ohm m, to superconductors $\varrho = 10^{-26}$ Ohm m.

If $\mathcal{R}$ corresponds to a conductor, the inductance term is small and only the induced EMF enters the equation, thus the intensity becomes $\mathcal{I}(z) \approx -\frac{1}{\mathcal{R}}\frac{\mathrm{d}\Phi}{\mathrm{d}t} = \frac{V(z)}{\mathcal{R}}$ and therefore, from Eqs. (1) and (19), we get for one coil

$$\mathcal{I}_1(z) = \frac{12}{\pi}\frac{\mathcal{M}\,\gamma\,v\,A\,z}{\mathcal{R}}\frac{1}{\left(z^2+\frac{A}{\pi}\right)^{5/2}} = \frac{12}{\pi}\frac{\mathcal{M}\,\gamma\,v\,A\,z}{\mathcal{R}}\frac{1}{(z^2+R^2)^{5/2}}, \tag{22}$$

and for the solenoid

$$\begin{aligned}\mathcal{I}_N^{\mathrm{in}}(z) &= -0.4576\,\frac{\mathcal{M}\,\gamma\,v\,A^2\,N}{\mathcal{R}}\frac{1}{(z^2+2R^2)^{5/2}},\\ \mathcal{I}_N^{\mathrm{out}}(z) &= +0.4576\,\frac{\mathcal{M}\,\gamma\,v\,A^2\,N}{\mathcal{R}}\frac{1}{((z-L)^2+2R^2)^{5/2}}.\end{aligned} \tag{23}$$

If $\mathcal{R}$ corresponds to a superconductor, then the term $\mathcal{I}\mathcal{R}$ is negligible and the intensity is given by $\mathcal{I}(z) = -\frac{\Phi}{\mathfrak{L}} = \frac{1}{\gamma\,v\,\mathfrak{L}}\int_{-\infty}^{z} V(z)\,\mathrm{d}z$, which becomes for the single coil

$$\mathcal{I}_1 = \frac{4}{\pi}\frac{\mathcal{M}A}{\mathfrak{L}}\frac{1}{(z^2+\frac{A}{\pi})^{3/2}} = \frac{4}{\pi}\frac{\mathcal{M}A}{\mathfrak{L}}\frac{1}{(z^2+R^2)^{3/2}}, \tag{24}$$

and for the N coil solenoid,

$$\begin{aligned}\mathcal{I}_N^{\mathrm{in}}(z) &= -\frac{0.4576}{\mathfrak{L}}\,\mathcal{M}\,A^2\,N\int_{-\infty}^{z}\frac{1}{\left(z^2+\frac{2A}{\pi}\right)^{5/2}}\,\mathrm{d}z\\ &= -\frac{0.3762}{\mathfrak{L}}\,\mathcal{M}\,N\,\frac{z(3R^2+z^2)}{(z^2+2R^2)^{3/2}},\\ \mathcal{I}_N^{\mathrm{out}}(z) &= \frac{0.4576}{\mathfrak{L}}\,\mathcal{M}\,A^2\,N\int_{-\infty}^{z}\frac{1}{\left((z-L)^2+\frac{2A}{\pi}\right)^{5/2}}\,\mathrm{d}z\\ &= \frac{0.3762}{\mathfrak{L}}\,\mathcal{M}\,N\frac{(z-L)(3R^2+(z-L)^2)}{((z-L)^2+2R^2)^{3/2}}.\end{aligned} \tag{25}$$

Let us study first the case of conducting coils, i.e., $\mathcal{R} \neq 0$ for stable particles. The energy our detector can extract from the flux of dipoles is the integral of the power in time

$$\mathcal{E} = \int_{-\infty}^{+\infty}\frac{V^2(t)}{\mathcal{R}}\,\mathrm{d}t. \tag{26}$$

Thus, for the single coil, the integral is immediate and we get

$$\mathcal{E} = \left(\frac{12}{\pi}\right)^2\frac{\mathcal{M}^2\gamma v\,A^2}{\mathcal{R}}\int_{-\infty}^{+\infty}\frac{z^2}{\left(z^2+\frac{A}{\pi}\right)^5}\,\mathrm{d}z = \frac{45}{8\pi}\frac{\mathcal{M}^2\gamma v}{R^3\mathcal{R}}. \tag{27}$$

For the solenoid, the integral expression is

$$\mathcal{E} \sim 0.2094\frac{\mathcal{M}^2\,\gamma\,v\,A^4\,N^2}{\mathcal{R}}\int_{-\infty}^{+\infty}\left(\frac{1}{(z^2+\frac{2A}{\pi})^{5/2}}+\frac{1}{\left((z-L)^2+\frac{2A}{\pi}\right)^{5/2}}\right)^2\mathrm{d}z, \tag{28}$$

and its integration requires some discussion.

The integral of the square terms can be performed analytically while the cross term not. In any case, all of the three terms are very convergent, and numerically we can get the result quite fast. However, the square terms tend to be much larger than the cross term, specially if L is large compared to the width of the potential bumps, since the cross term only takes into account the overlap between the bumps. This argument has been checked numerically for the scenarios of the present calculation, and therefore, we neglect safely the cross term and get an analytic result which is

$$\begin{aligned}\mathcal{E} &\sim 0.2094\frac{\mathcal{M}^2\,\gamma\,v\,A^4\,N^2}{\mathcal{R}}\frac{35\pi}{64}\left(\frac{2A}{\pi}\right)^{-9/2}\\ &\sim 2.7451\frac{\mathcal{M}^2\,\gamma\,v\,N^2}{\mathcal{R}\sqrt{A}}.\end{aligned} \tag{29}$$

If we use the following units $\mathcal{M}$ (fm), v in units of the velocity of light in the vacuum, S (mm^2), R (mm) and ϱ (Ohm m), the equation for the energy becomes for the single coil

$$\mathcal{E} = 0.1660\,10^{-28}\,\frac{\mathcal{M}^2\gamma v\,S}{R^4\varrho}\ \mathrm{eV}\,, \tag{30}$$

and for the solenoid,

$$\mathcal{E} = 0.1455\,10^{-29}\,\frac{\mathcal{M}^2\,\gamma\,v\,S\,N}{R^2\,\varrho}\ \text{eV}\,. \tag{31}$$

Let us now study the case of superconducting coils where the inductance term is dominant. In this case,

$$\mathcal{E} = \frac{\mathfrak{L}}{2}\int_{-\infty}^{+\infty}\frac{\mathrm{d}\mathcal{I}_N^2(t)}{\mathrm{d}t}\,\mathrm{d}t = \frac{\mathfrak{L}}{2}\left((\mathcal{I}_N^{\text{in}})^2(+\infty) + (\mathcal{I}_N^{\text{out}})^2(+\infty)\right) = 0.1415\,\frac{\mathcal{M}^2\,N^2}{\mathfrak{L}} \tag{32}$$

For a thin long solenoid, the ratio of inductance for superconducting and normal solenoids is close to 1 [22], thus $\mathfrak{L} = \mu_0\frac{N^2A}{L}$ where $\mathfrak{L}$ is in H, if we take $\mu_0 = 4\pi\,10^{-7}$ H/m , A is the area of the coil in m^2, L is the length of the coil in m. Recall that $H =$ Ohm s, then

$$\mathcal{E} = 0.2486\,10^{-16}\,\frac{\mathcal{M}^2L}{R^2}\ \text{eV}\,. \tag{33}$$

where we are measuring $\mathcal{M}$ in fm, R in mm and L in m. This choice of three units might seem strange at first, but it is related to the natural scale of the physics and the apparatus: The magnetic moments of the states of monopolium are microscopic (0–1000 fm), the most effective coils are of millimeters size (0.01–1 mm) , and in order to have very large number of coils, we need solenoids lengths of meters.

The behavior of Eqs. (31) and (33) is very different. For the former, the parameters at our disposal to increase the sensibility of the detector are the number of coils N, the velocity of the dipole v, but specially the factor γ, the radius of the coil R and the resistivity of the material ϱ. For the latter, the length of the solenoid L and the radius of the coil R but neither the velocity nor the number of coils play a role.

3.2 Application to particles with finite lifetime

In the previous subsections, we have considered the effect on coils of permanent magnetic moments. Here, we modify our formulation to magnetic moments of particles with finite lifetime. By generalizing Eq. (27) to this case, we get for the energy stored in one coil during the lifetime of particle

$$\begin{aligned}\mathcal{E} &\sim \left(\frac{12}{\pi}\right)^2\frac{\mathcal{M}^2\gamma\,v\,A^2}{\mathcal{R}}\int_{-z}^{+z}\frac{z^2}{\left(z^2+\frac{A}{\pi}\right)^5}\,\mathrm{d}z\\ &\sim \frac{144\,\mathcal{M}^2\gamma\,v}{\mathcal{R}R^3}\int_{-a}^{+a}\frac{y^2}{(y^2+1)^5}\,\mathrm{d}y\\ &\sim 0.1353\,10^{-28}\frac{\mathcal{M}^2\gamma\,vS}{R^4\varrho}\mathcal{F}(a)\ \text{eV}\,.\end{aligned} \tag{34}$$

where $a = \frac{z}{R}$, z is half the distance traveled during the particles lifetime, v is the velocity of the state, γ is the corresponding relativistic factor, $\mathcal{M}$ is the magnetic moment, $\mathcal{R}$ is the resistance of the coil and R is the coil radius and S is the surface section of the resistor. The integral in Eq. (34) $\mathcal{F}(a)$ can be solved analytically giving

$$\mathcal{F}(a) = \int_{-a}^{+a}\frac{y^2}{(y^2+1)^5}\,\mathrm{d}y = \frac{1}{192}\left(\frac{15a^7+55a^5+73a^3-15a}{(1+a^2)^4}+15\arctan a\right). \tag{35}$$

We are assuming that the coil is located in the center of the path traveled by the particle during its lifetime. If this path is large compared with the radius of the coil, this is not a bad approximation given the behavior of $\mathcal{F}(a)$. If we put N coils next to each other but sufficiently separated that there is no interaction between them, we have to multiply Eq. (34) by N.

We proceed analogously with the solenoid, and in order to get an analytic formula, we make the same approximation as before, namely we disregard the cross term, the result is

$$\begin{aligned}\mathcal{E} &\sim 0.2094\frac{\mathcal{M}^2\gamma_n\,v_n\,A^4N^2}{\mathcal{R}}\left(\int_{-z}^{+z}\frac{1}{\left(z^2+\frac{2A}{\pi}\right)^5}\,\mathrm{d}z+\int_{-z}^{+z}\frac{1}{\left((z-L)^2+\frac{2A}{\pi}\right)^5}\,\mathrm{d}z\right)\\ &\sim\ 0.1435\frac{\mathcal{M}^2\gamma\,v\,SN}{R^2\varrho}\left(\int_{-b}^{+b}\frac{1}{(y^2+1)^5}\,\mathrm{d}z+\int_{-b}^{+b}\frac{1}{((y-l)^2+1)^5}\,\mathrm{d}z\right)\\ &\sim 0.8469\,10^{-30}\frac{\mathcal{M}^2\gamma\,v\,SN}{R^2\varrho}(\mathcal{G}(b)+\frac{1}{2}\mathcal{G}(b-l)+\frac{1}{2}\mathcal{G}(b+l))\ \text{eV}\end{aligned} \tag{36}$$

where $b = \frac{z}{\sqrt{2}R}$, $l = \frac{L}{\sqrt{2}R}$ and the integrals can be expressed in terms of the function

$$\mathcal{G}(b) = \frac{1}{192}\left(\frac{105b^7+385b^5+511b^3+279b}{(1+b^4)^2}+105\arctan b\right). \tag{37}$$

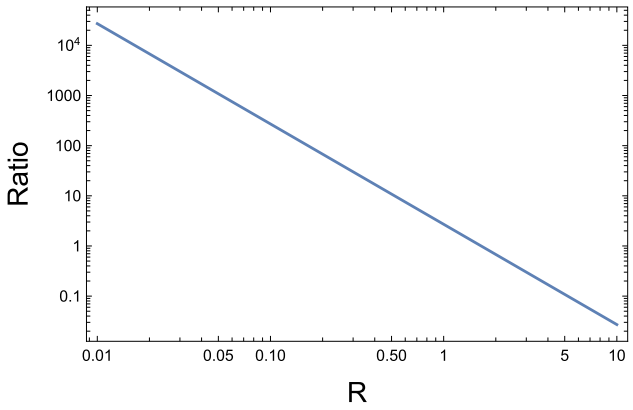

Fig. 6 We show the ratio of a coil system with respect to a solenoid. The ratio is almost independent on the number of coils as long as they are the same and $z > R$

The formulation just described can be applied to any particle with a finite lifetime with magnetic moment and no charge.

In order to choose the best parameters, we show in Fig. 6 the ratio of the effect of N separated coils with respect to a N coils solenoid for large N. The dependence of the coil radius and the coil section is crucial. We choose the radius of the coil section r_s for technical reasons about $r_s \sim 0.01R$. The figure shows that for large radii $R > 2$ mm, the solenoid is more efficient, while for microcoils $R < 2$ mm, the coil system is more efficient. We shall use in what follows microcoils $R \sim 0.01$ mm and $r_s \sim 0.0001$ mm and therefore N coil systems instead of solenoids.

3.3 Effect of the induced current on the velocity of the particle

One might wonder if the induced current through the inductance can produce an effect contrary to the one just discussed which reduces the signal significantly. For simplicity, we will perform a non-relativistic calculation which is very transparent. Let us assume a particle traveling with constant velocity toward a conducting coil with its magnetic dipole moment perpendicular to the plane of the coil as shown in Fig. 1. We would like to find out the motion of this particle due to the effect of the Faraday-Lenz law which creates a magnetic field $\vec{B} = B_z\hat{k}$ where

$$B_z = \frac{2\pi R^2 \mathcal{I}}{(z^2 + R^2)^{3/2}}, \tag{38}$$

with $\mathcal{I}$ the intensity of the current running through the coil, z is the distance from the particle to the center of the coil and R is the coil radius. Newtons's equation for the problem is given by

$$M\frac{\mathrm{d}^2 z}{\mathrm{d}t^2} = -\mathcal{M}\frac{\mathrm{d}B_z}{\mathrm{d}z}. \tag{39}$$

In order to get the intensity, we use Ohm's law Eq. (21) and the magnetic flux Φ given by Eq. (8). Since we are dealing with a very good conductor, $\mathcal{R} = \frac{2\pi R}{\pi r_s^2}\varrho$, where r_s is the radius of the conductor and ϱ the resistivity $\varrho = 10^{-8}$ Ohm m and has a small inductance $\mathcal{L} = 0.1$ nH. Thus, the set of equations that determine the motion of the particle are

$$M\frac{\mathrm{d}^2 z}{\mathrm{d}t^2} = -6\pi\mathcal{M}R^2\mathcal{I}\frac{z}{(z^2 + R^2)^{3/2}}, \tag{40}$$

$$\mathcal{L}\frac{\mathrm{d}\mathcal{I}}{\mathrm{d}t} + \mathcal{I}\mathcal{R} = 6\pi\mathcal{M}R^2\mathcal{I}\frac{z}{(z^2 + R^2)^{3/2}}\frac{\mathrm{d}z}{\mathrm{d}t}. \tag{41}$$

This is a system of differential equations for $z(t)$ and $\mathcal{I}(t)$ which has to be solved simultaneously. The initial conditions will be z_i, v_i and $\mathcal{I}_i$. We shall take z_i sufficiently far from the coil so that the induced current is very small initially. The parameters that influence the solution are $\mathcal{L}$, $\mathcal{R}$, $\mathcal{M}$ and v_i. The outcome of our calculation is shown in Fig. 7.

As can be seen in Fig. 7, the particle approaches the coil at large distances without changing its velocity. Close to the coil, for large $\mathcal{M}$, the velocity drops due to an acceleration opposite to the direction of motion associated to the creation of an induced current. Due to the variation in the current, the inductance term becomes active and generates an acceleration opposite to the one generated before, which increases the velocity slightly and therefore decreases the current. Finally, the Ohm term dominates over the inductance term and the velocity is decreased again and the current increases, until the particle leaves the region of influence of the coil with a smaller velocity and stops to generate current. The figure corresponds to the solution of the equations for $z_i = -10$ mm, $v_i = 7.\,10^{-5}$, $t = 10^{-6}$ s, and a very high lying Rydberg state with $\mathcal{M} \sim 300$ fm. The effect of the inductance term on the velocity is very small, and the full change of the velocity by the coil is also small so that the position has a negligible kink at the origin. In this case, the velocity changes from $2.1\,10^7$ mm/s to $2.099999985\,10^7$ mm/s, and if we follow the initial trajectory beyond the coil $z_-(0.6\,10^{-6}) = 2.6$ cm, while the position the particle follows after the coil is $z_+(0.6\,10^{-6}) = 2.59999998$ cm.

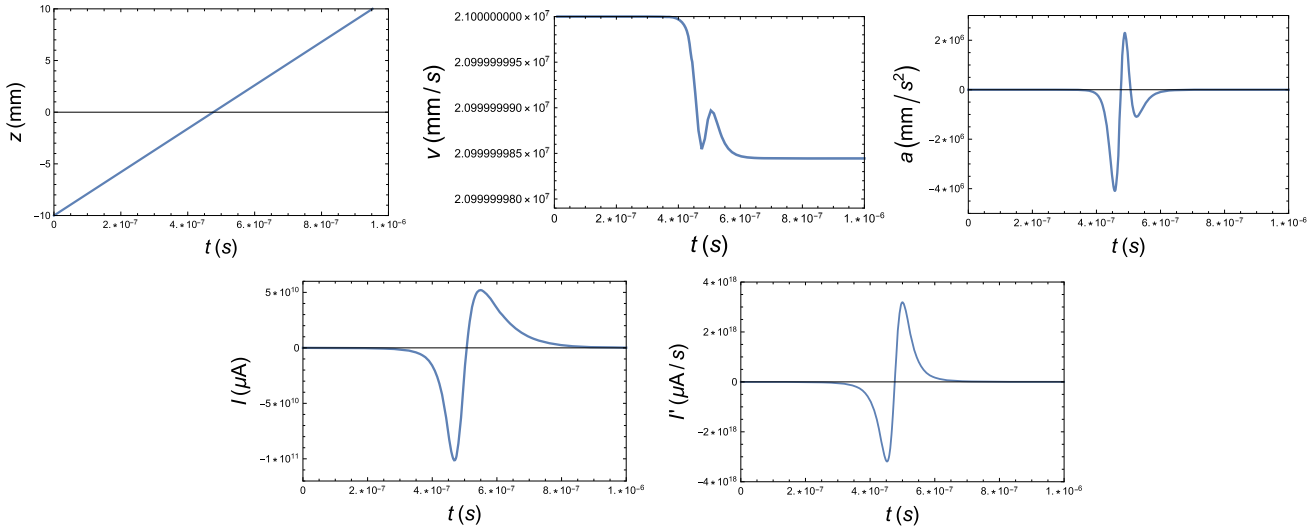

Fig. 7 A high excited monopolium ($\mathcal{M} \sim 300$ fm) traveling with constant velocity ($v = 7\ 10^{-5}$) from $z_i = -10$ mm toward a conducting coil located at $z = 0$ with its magnetic dipole moment perpendicular to the plane of the coil. The upper figures from left to right show variation in the position, velocity and acceleration with time. The lower figure show the variation in the induced current and its derivative with time

The conclusion of this analysis is twofold: On the one hand, the induced current does not influence significantly the calculation, and from now on, we shall not take the induction effect into consideration; on the other hand, the effect of the coil on the velocity is small. Despite this, given the large mass of the monopolium states, the created current is not negligible.

4 Analysis of monopolium properties using coils and solenoids

We proceed to apply the coil effect to monopolium a monopole-antimonopole bound state and its excitations. We proceed to discuss two experimental scenarios of monopolium: one related to a relatively light monopolium ($M \sim$ TeVs) which can be created by particle collisions [10, 23] and one related to a heavy monopolium ($M \sim M_{\rm GUT}$ and $M \sim M_{\rm Planck}$) that might be created in cosmological scenarios [6, 14].

4.1 Low mass monopolium

Let us review some properties of monopolium which are useful for the calculation of low mass monopolium. There are several models in the literature to describe the monopole-antimonopole potential in monopolium [24–28]. For the purpose of our present investigation, the analytic approximation to the potential of Schiff [24] and Goebel [25]

$$V(r) = -g^2 \frac{1 - \exp(-2r/r_0)}{r}, \tag{42}$$

used in Refs. [29, 30] will be sufficient. The approximation consists in substituting the true wave functions by Coulomb wave functions of high n. For each r_0 in Eq. (42), a different value of n will be best suited. We use the equation

$$\rho_n = 48\alpha^2 n^2, \tag{43}$$

to parametrize all expectation values in terms of ρ_n, where $\rho_n = r_M / r_{\rm classical}$, r_M, being the radius of the monopolium state, $r_{\rm classical}$ is the classical magnetic radius of the monopole g^2/m, α is the electromagnetic fine structure constant. This relation results from the calculation of the expectation value of r in the $(n, 0)$ Coulomb state.

We determine an approximate wave function for the ground state of the Schiff–Goebel potential in terms of a Coulomb wave function with a $n_{\rm min}$. In terms of $\rho_{n_{\rm min}}$, the mass of ground state monopolium becomes [29, 30]

$$M = m\left(2 - \frac{3}{4\rho_{n_{\rm min}}}\right). \tag{44}$$

Thus, given a monopole mass m and a monopolium ground state mass M, we determine $\rho_{n_{\rm min}}$ which determines $n_{\rm min}$. The binding energy of the ground state is thus $E_{n_{\rm min}} = \frac{3m}{4\rho_{n_{\rm min}}}$. The excited states correspond to $n > n_{\rm min}$. Let us label the excited states only by

their principal quantum number n since we are assuming in our simple Coulomb potential model that all the l corresponding to an n are degenerate, thus their mass would be

$$M_n = m\left(2 - \frac{3}{4\rho_n}\right), \tag{45}$$

and their binding energy $E_n = \frac{3m}{4\rho_n}$. The high lying deformed ($l \neq 0$) states will have a larger magnetic moment and a larger size. Recall that in a Coulomb like potential

$$\frac{\langle nl|r|nl\rangle}{r_{\text{Bohr}}} \sim \left(\frac{3}{2}n^2 - \frac{1}{2}l(l+1)\right) \sim n^2, \tag{46}$$

an approximation valid for large l. Thus, the high lying states will increase their size approximately as n^2. These states will be called Rydberg states following the atomic nomenclature. For them, given their large size, the Schiff–Goebbel wave functions reduce to the Coulomb wave functions.

We estimate the magnetic moment of the Rydberg sates as

$$\mathcal{M}_n \sim g\,\langle nl|r|nl\rangle = g\,\rho_n\, r_{\text{classical}} = \frac{3}{32\,\alpha^{3/2}\,E_n}, \tag{47}$$

where we have used the Dirac quantization condition (DQC) $g\,e = \frac{1}{2}$ and $r_{\text{classical}} = g^2/\text{m}$. Looking at Eq. (47), it is clear that Rydberg states will have the largest magnetic moments.

The two photon decay width of the monopolium excited states is determined by [10, 30]

$$\Gamma_n^{2ph}(E) = \frac{2\,\beta_n^4\,m^3}{\alpha^2 M_n^2}\left(\frac{E_n}{m}\right)^{3/2}. \tag{48}$$

At leading order, the dominant decay rates are determined by the two photon width, Eq. (48), which depends on the wave function at the origin, and is only nonzero for S ($l = 0$) states. The $l \neq 0$ states arise by de-excitation to lower n levels. The decay rate for the S states goes like $1/n^3$ [31, 32].

Our interest here lies in the high lying deformed Rydberg states which are in high l states, with vanishing wave function at the origin, that is to say that the monopole and antimonopole are far away from each other and therefore do not annihilate as it is the case for positronium. They will de-excite by spontaneous emission of photons to the lower levels where they will annihilate either as S states or to non-leading order as $l \neq 0$ state decays. In order to get an estimate for spontaneous emission as a function of n, we use the Larmor radiation formula applied to the naive Bohr model [33],

$$\Gamma_n^{se}(E) = \frac{512}{3}\,\beta_n^4\,\alpha\,m\left(\frac{E_n}{m}\right)^3. \tag{49}$$

Note that, this dependence goes like $1/n^6$, therefore lifetimes of these Rydberg states increase notably with n.

Two coupling schemes have been used in the literature: The Dirac coupling scheme [1, 2] is characterized by point-like monopoles which couple with magnetic charge g, while the β or Schwinger scheme [34] is characterized by a monopole coupling of magnetic charge βg, where β is the velocity of the monopole. In Eqs. (48) and (49), $\beta_n = 1$ for Dirac coupling and $\beta_n = v_n$ for Schwinger coupling, where v_n is the velocity of the monopolium state, α is the fine structure constant, which appears after using the DQC and m stands for the monopole mass.

Let us next specify the properties of monopolium excited states when passing through coils in each of these schemes.

4.1.1 The Dirac coupling scheme

The states with the largest magnetic moment, i.e., the most deformed states will be Rydberg states with very small binding energy, $E_n << 2m$. The distance traveled by monopolium with binding energy $E_n = \frac{m}{64\alpha^2\,n^2}$ for high n before decaying is

$$d_n = \frac{\gamma_n\,v_n}{\Gamma_n^{se}} \sim \frac{3}{512}\,\frac{\gamma_n\,v_n}{\alpha\,m\left(\frac{E_n}{m}\right)^3}, \tag{50}$$

since spontaneous emission dominates to annihilation for high n. In Fig. 8, we show d_n as a function of the binding energy E_n for Rydberg states made of mass $m \sim 1$ TeV for different velocities (left), and for fixed velocity (0.99) for Rydberg states made of monopoles of different masses (right). As can be immediately seen from Eq. (50), the distance from production to annihilation grows naturally as the velocity increases and also grows as the mass is increased, because the dependence on the mass is dominated by the lifetime. Moreover, the curve diverges for $E_n \to 0$, i.e., $n \to \infty$ indicating that for small binding energies, the distance traveled by monopolium before decaying can be very large if the system does not breakup by external interactions.

Let us now look at our signal which is the deposited energy calculated from Eqs. (34) and (35). In Fig. 9, we show $\mathcal{E}_n$ for Rydberg states made of monopoles of mass 1 TeV as a function of the binding energy E_n in eV, for a coil system with 10^8 coils, with

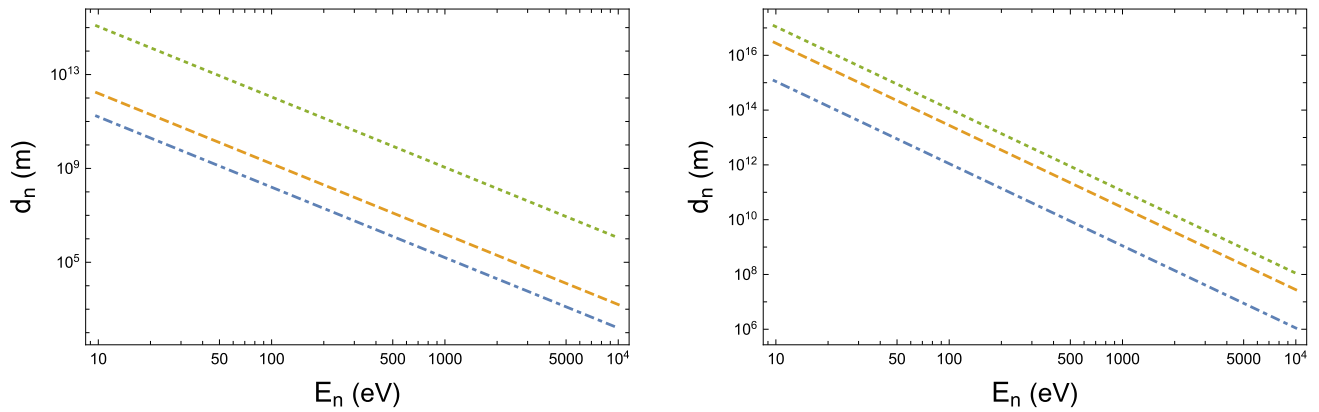

Fig. 8 Distance traveled by monopolium in meter as a function of binding energy E_n in eV before decaying. Left: for fixed monopole mass $m = 1$ TeV and three different velocities 0.001 (dotdashed), 0.01 (dashed) and 0.99 (dotted). Right: for fixed velocity 0.99 and three masses 1 TeV (dotdashed), 5 TeV (dashed) and 10TeV dotted

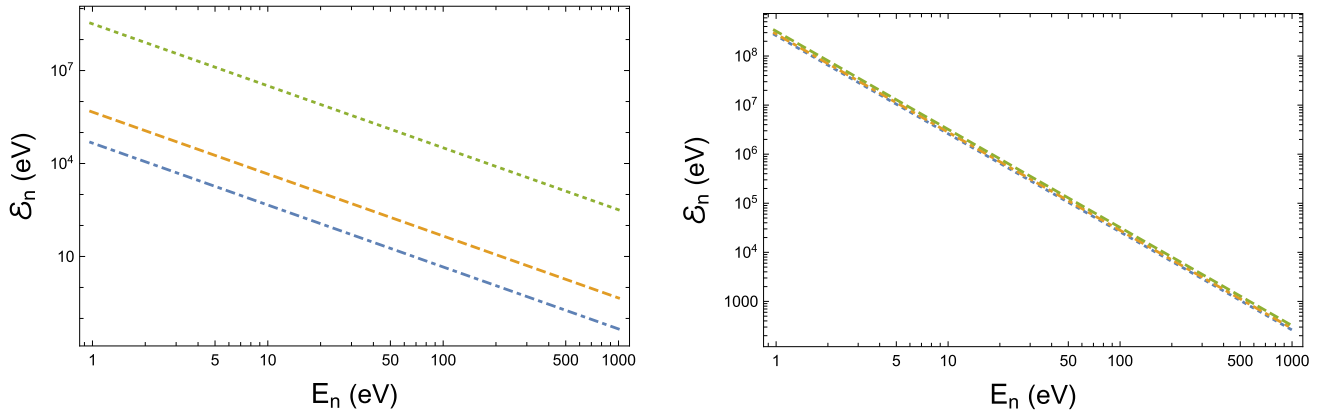

Fig. 9 Energy deposited in a coil system with 10^8 coils by the passing of a monopolium Rydberg state n as a function of binding energy E_n (eV) . Left: for fixed monopoles mass $m = 1$ TeV and three different velocities 0.001 (dotdashed), 0.01 (dashed), 0.99 (dotted). Right: for fixed velocity 0.99 and monopole masses 1 TeV (dotdashed), 5 TeV (dashed) and 10 TeV (dotted). The three curves are the same, we have separated them by using slightly different velocities

$\mathcal{R} = \frac{2\pi R\varrho}{\pi r_s^2}$, where the radius of the coils is $R = 0.01$ mm, the radius of the section of the coils is $r_s = 0.0001$ mm, the resistivity $\varrho = 10^{-8}$ Ohm m, and for three velocities 0.001, 0.01 and 0.99 (left), and the same for fixed velocity 0.99 and for Rydberg states made of monopoles of different masses. The coil system is defined by coils separated $2r_s$ from the next coil. 10^8 coils define a coil system of 40 m. The interesting result is that the deposited coil energy for a fixed binding energy does not depend on the mass. To understand this, we have to recall that the binding energy is proportional to m and inversely proportional to n^2, thus the states for the same binding energy and different masses the value of n changes. Thus, the higher the monopole mass, the higher has to be the Rydberg state in order to have the same binding energy.

4.1.2 The Schwinger coupling scheme

The velocity in Eq. (49) in Schwinger coupling makes the lifetime very long at threshold, and therefore, we expect some interesting physics around the threshold region. Away from threshold, both Dirac and Schwinger coupling schemes coincide. Let us calculate the value of d_n at threshold

$$\lim_{E_n^{\rm tot}\to M_n} d_n(E_n^{\rm tot}) \sim \frac{3}{512}\frac{m^2}{\alpha\, E_n^3}\left(\frac{M_n}{2(E_n^{\rm tot}-M_n)}\right)^{3/2} \sim \frac{3}{512}\frac{m^2}{\alpha\, E_n^3\, v_n^3} \tag{51}$$

The distance traveled by monopolia diverges at threshold as shown in Fig. 10. $E_n^{\rm tot} = \gamma_n M_n$ is the total energy of the Rydberg state, M_n being its mass. In this case, the distance traveled decreases with increasing velocity due to the beta coupling in the width of the state. With respect to the monopole mass dependence, the traveled distance increases since the lifetime of the state increases.

In Fig. 11, we compare the results for Schwinger and Dirac schemes, noting the different behavior of the dependence with velocity, confirming that close to threshold, the lifetimes are very different, while as the velocity increases, their behavior becomes similar.

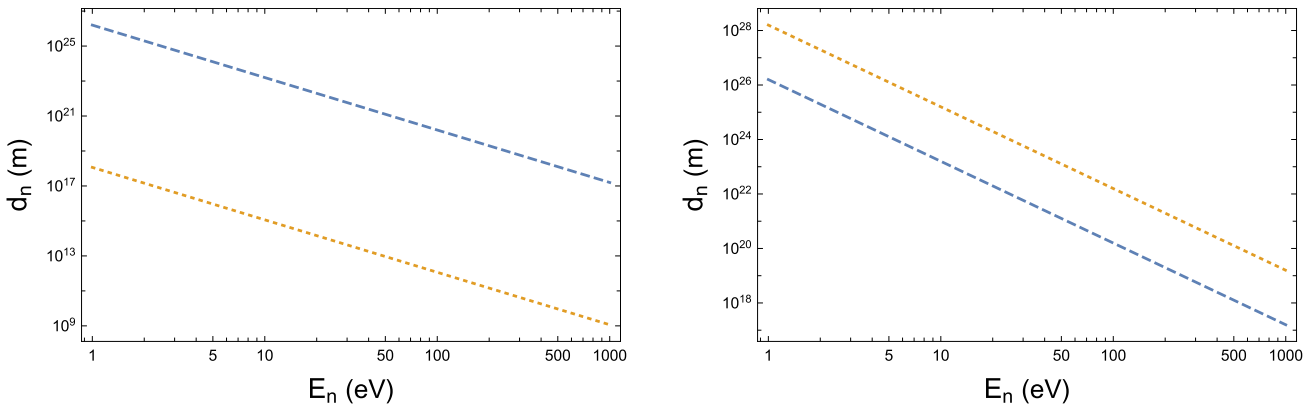

Fig. 10 The left figure shows the distance traveled by an excited state of monopolium as a function of binding energy for Schwinger coupling close to threshold $v_n \sim 0.001$ (dashed) and $v_n = 0.99$ (dotted) and monopole mass 1 TeV. The right figure shows the same for fixed velocity 0.001 and monopole masses 1 TeV (dashed) and 10 TeV (dotted)

Fig. 11 The distance traveled by a Rydberg state of binding energy 10 eV as a function of velocity both for Schwinger coupling (dashed) and for Dirac coupling (dotted)

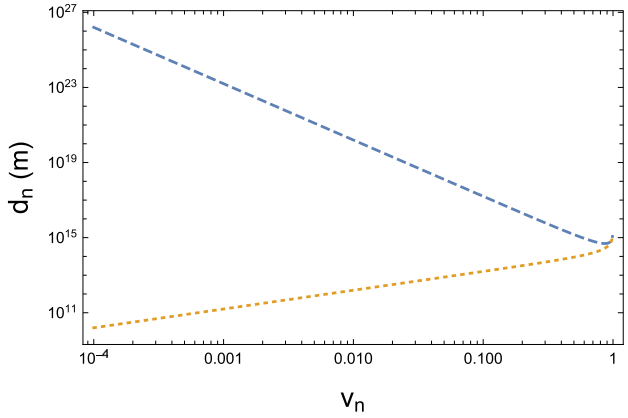

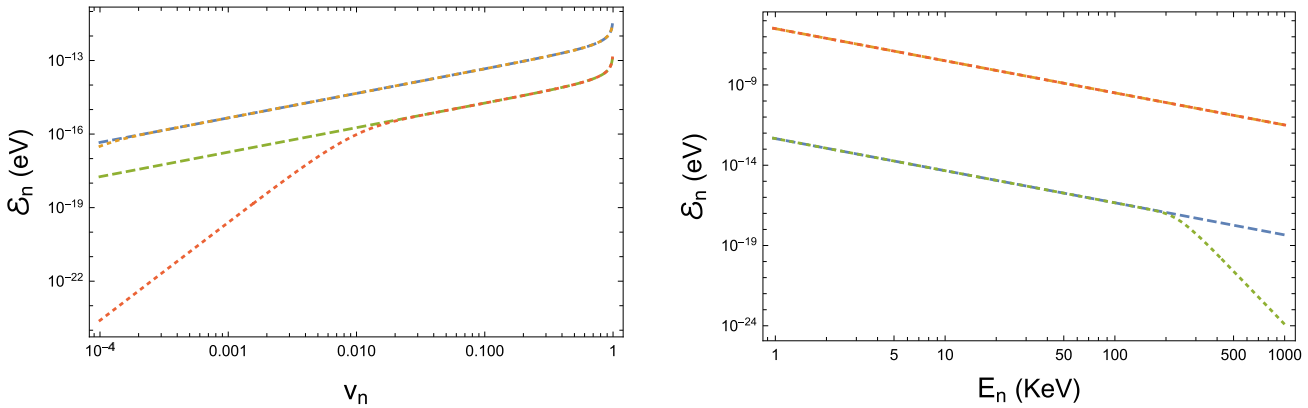

Fig. 12 Left: we show the variation in the deposited energy with velocity in one coil for fixed binding energy $En = 1000$ KeV in the Schwinger scheme (dashed) and in the Dirac scheme (dotted) and for $E_n = 5000$ KeV in the Schwinger scheme (dashed) and in the Dirac scheme (dotted). Right: we show the variation in the deposited energy in one coil with binding energy $E_n = 1000$ KeV for fixed velocity $v_n = 0.00001$ close to threshold in the Schwinger scheme (dashed) and in the Dirac scheme (dotted) and for $v_n = 0.99$ away from threshold in the Schwinger scheme (dashed) and in the Dirac scheme (dotted). The monopole mass used in both calculations is 1 TeV

The threshold behavior for the deposited energy can be calculated analytically from Eqs. (34) and (35) using that at threshold $a_n \sim \frac{d_n}{2R} \to \infty$, therefore $\mathcal{F}(a_n) \to \frac{5\pi}{128}$, we get

$$\lim_{E\to M_n} \mathcal{E}_n \sim 0.1353\, 10^{-28} \frac{\mathcal{M}_n^2 \gamma_n v_n SN}{R^4 \varrho} \mathcal{F}(a_n) \sim 0.2348\, 10^{-29} \frac{\mathcal{M}_n^2 SN}{R^4 \varrho} \left(\frac{E_n^{\rm tot} - M_n}{E_n^{\rm tot}} \right)^{1/2} \sim 0.1660\, 10^{-29} \frac{\mathcal{M}_n^2 SN}{R^4 \varrho} v_n \quad \text{eV} . \quad (52)$$

The linear behavior with the velocity appears clearly in the exact numerical calculations of Fig. 12, where we show the behavior of the deposited energy for fixed binding energy and varying velocity (left) and for fixed velocity and varying binding energy

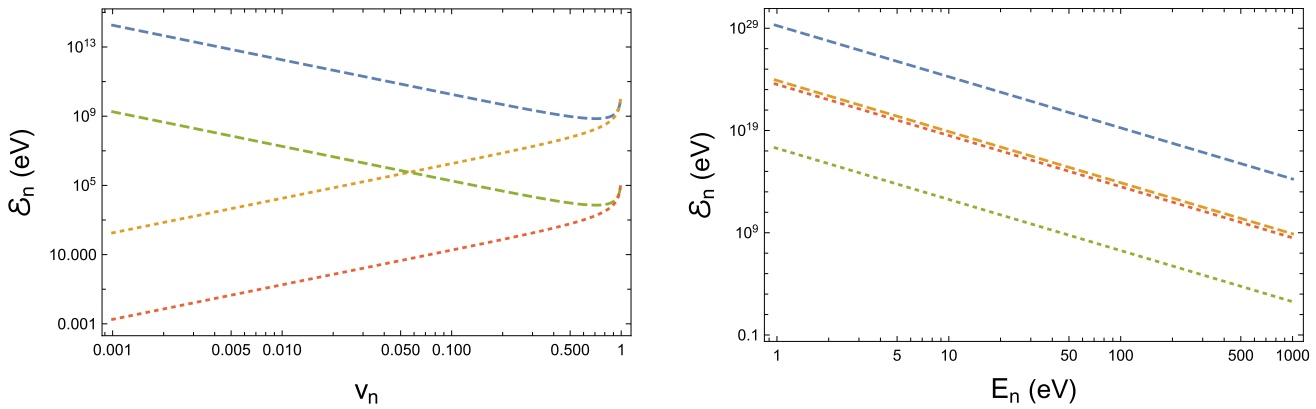

Fig. 13 Left: we show the variation in the deposited energy with velocity in the maximal coil system for fixed binding energy $E_n = 1$ KeV in the Schwinger scheme (dashed) and in the Dirac scheme (dotted) and for $E_n = 10$ KeV in the Schwinger scheme (dashed) and in the Dirac scheme (dotted). Right: we show the variation in the deposited energy in the maximal coil system with binding energy E_n for fixed velocity $v_n = 0.001$ close to threshold in the Schwinger scheme (dashed) and in the Dirac scheme (doted) and for $v_n = 0.8$ away from threshold in the Schwinger scheme (dashed) and in the Dirac scheme (dotted). When the velocity approaches $v_n \sim 1$, the Schwinger and the Dirac scheme coincide. The monopole mass used in both calculations is 1 TeV

(right) in both Schwinger and Dirac schemes. We note that in the Schwinger scheme, the linear velocity dependence ceases at large velocities, while in the Dirac scheme, the behavior at threshold is not linear. However, for small binding energies, the behavior of the two schemes is dominated by the binding energy whose behavior is the same. This leads to the superposition of the dashed curve (Schwinger) to the dotted curve (Dirac) for small binding in the figure on the left and for small binding and small velocity in the figure on the right. For high binding energies and small velocities, the two schemes tend to deviate considerably as can be seen in the figure on the right. Note that, in the Schwinger scheme, also the deposited energy grows as the velocity increases as happens in the Dirac scheme.

For small binding energies, there is not much difference in the deposited energy for both schemes if both traverse the coil system. The main difference between the Schwinger scheme and the Dirac scheme lies in Fig. 10, namely that the chance for a Schwinger monopolium to reach a detector is greater because it lives longer and that it can traverse longer coil systems. This behavior is explicit in Fig. 13 where we are assuming that monopolium is created at the beginning of the coil system and it traverses a coil system of length d_n. In this case, we see how the behavior with velocity changes for Schwinger coupling, namely the deposited energy decreases with velocity because the distance traveled by monopolium before decaying becomes smaller, and the detector has less coils. The contrary happens for the Dirac scheme. The behavior with binding energy is the same in both cases, only that the effect for Schwinger coupling is much bigger for small velocities because the number of coils is larger. In the limit of large velocities, both schemes become equal.

Given the reachable luminosities at LHC, Rydberg states on the scale of eV–KeV, which could lead to measurable deposited energies and lifetimes sufficiently long to escape the beam, cannot be produced and therefore we have to resort to cosmological scenarios [41].

5 Cosmic monopolium

5.1 Cosmic light monopolium

In the case of the monopolia just studied, i.e., light monopolia ($M_n \sim$ TeVs), we have to generalize the calculation of their velocity in a galaxy and find a reasonable flux bound. Monopolia will interact with the cosmological magnetic field through their magnetic moment, thus the force acting on them will be given by

$$\vec{F} = -\vec{\mathcal{M}}_n \cdot \vec{\nabla}\vec{B}, \tag{53}$$

where $\mathcal{M}_n \sim g r_n$ is the magnetic moment, r represents the distance between the poles and $\vec{B}$ is the cosmological magnetic field,

$$\begin{aligned} B(R) = & \; B_0 \; \tanh\left(\frac{R - R_C}{R_1}\right) \exp\left(-\left|\frac{R - R_C}{R_0}\right|\right) \quad \text{for } R > 0, \\ = & -B_0 \; \tanh\left(\frac{R + R_C}{R_1}\right) \exp\left(-\left|\frac{R + R_C}{R_0}\right|\right) \quad \text{for } R < 0. \end{aligned} \tag{54}$$

In the left hand side of Fig. 14, the model for the magnetic field of a galaxy described in Eq. 54 is shown [14] and in the right hand side its gradient along the model galaxy.

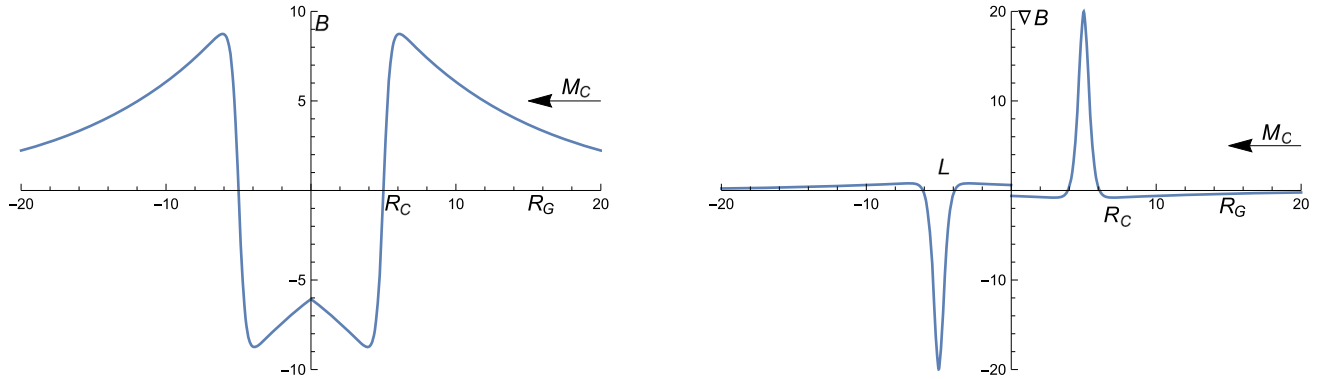

Fig. 14 Figure left: our one-dimensional model for the magnetic field of a galaxy. Figure right: magnetic field gradient of the model. M_C represents a monopolium cloud traveling toward the center of the galaxy

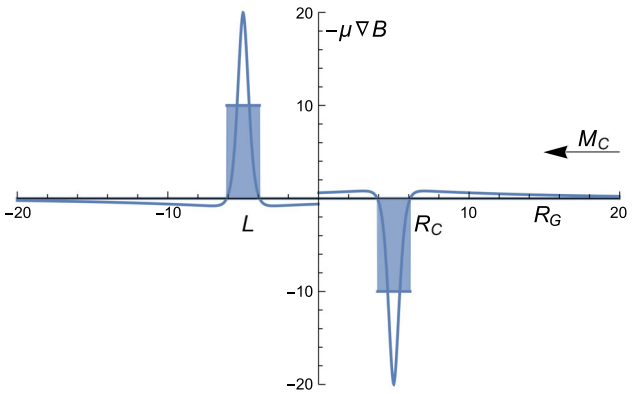

Fig. 15 The simplified force field used in the calculation of the velocity is in gray over imposed on the real force field. L is the width of the simplified force field

The mathematical structure of the field makes the analysis of the velocity of monopolium complicated. In order to get an estimate, we substitute the force field by two simplified forces of adequate strength as shown in Fig. 15 compared to the actual force field. With this constant force field the velocity becomes, after crossing the two accelerating structures, and using relativistic kinematics

$$v_n \sim \sqrt{1-\frac{1}{\left(\frac{g r_n B_0 L}{2 M_n R_1}+1\right)^2}} \sim \sqrt{1-\frac{1}{(0.32\,10^{-26}\,r_n+1)^2}}\,. \tag{55}$$

The last expression has been calculated for a high n Rydberg state, $M_n \sim 2000$ GeV, and for conventional values of the galaxy parameters $B_0 = 10\mu\text{G} \sim 1.95\ 10^{-25}\ \text{GeV}^2$, $R_1 = 0.5$ Kpc, where the width of the force field $L \sim 2.2$ Kpc, with r_n measured in fm. Despite the huge sizes of Rydberg states ($r_n \sim 10^9$ fm $\sim 10^{-3}$ mm), the small pre-factor in the formula cannot be overcome and the velocity originating from the gravitational magnetic fields will be much smaller than the galactic gravitational velocity $v_M \sim 10^{-3}$. The latter is mass independent [6].

The Rydberg states with long lifetimes and large magnetic moments are lightly bound monopole-antimonopole pairs with binding energies of the order of eVs and the small Parker bound, an upper bound on the density of magnetic monopoles [36], can be obviated and detection is possible [33]. The Parker bound is based on the monopoles taking energy from the intergalactic magnetic field. However, monopolia below the dissociation energy do not take energy from the magnetic field since they are almost neutral, i.e., magnetic moment interactions are much weaker than magnetic charge interactions.

The high lying Rydberg states might be dissociated by the much stronger Earth's magnetic field leading to free monopole-antimonopole pairs which might annihilate or ionize metal rods depending on its production kinematics. Monopolia below the Earth's dissociation limit survive and those close to the dissociation limit will have long lifetimes as shown in Fig. 16 and we expect them to be able to transverse long coil systems.

Let us calculate the minimum binding energy before dissociation by equating E_n with the dissociation energy [33]

$$E_n \sim g B_E r_n. \tag{56}$$

Using the $E_n = \frac{3m}{4\rho_n} = \frac{3g^2}{4r_n}$ and the Earth's magnetic field $B_E \sim 1$ G $\sim 1.95\,10^{-20}$ GeV^2, we get for the maximum allowed size $r_n \lesssim \sqrt{\frac{3}{8eB_E}} \sim 3.\,10^{-3}$ mm. For our light monopole $m \sim 10^3$ GeV, we obtain for the binding energy $E_n \gtrsim 1$ eV.

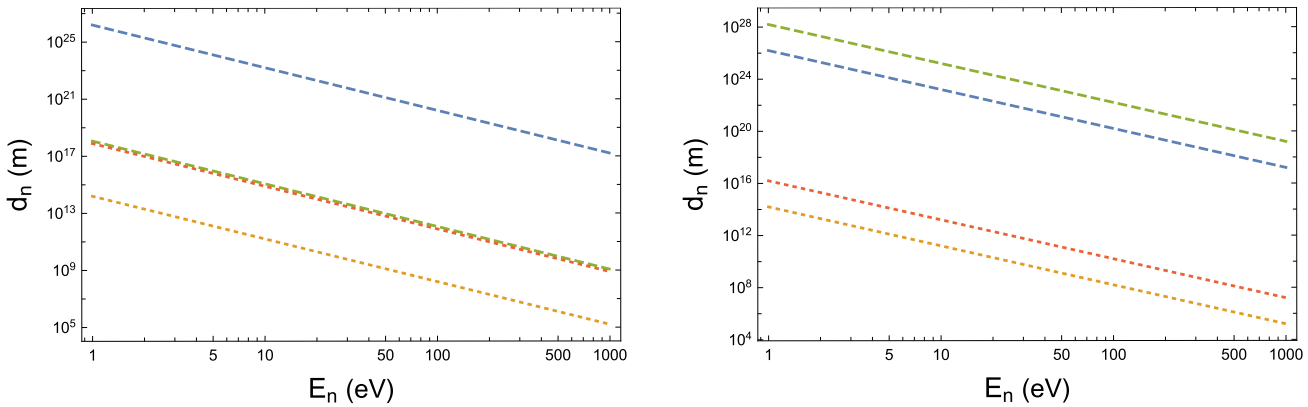

Fig. 16 We plot the distance traveled by monopolium Rydberg states before disintegrating as a function of binding energy for both Schwinger (dashed) and Dirac(dotted) schemes. Left figure for velocities 0.001 and 0.99 and fixed monopole mass of 1 TeV. Right figure for fixed velocity 0.001 and monopole masses 1 TeV and 10 TeV. We have used a velocity of 0.98 in the Dirac case to show that the two curves would superimpose for equal high velocity

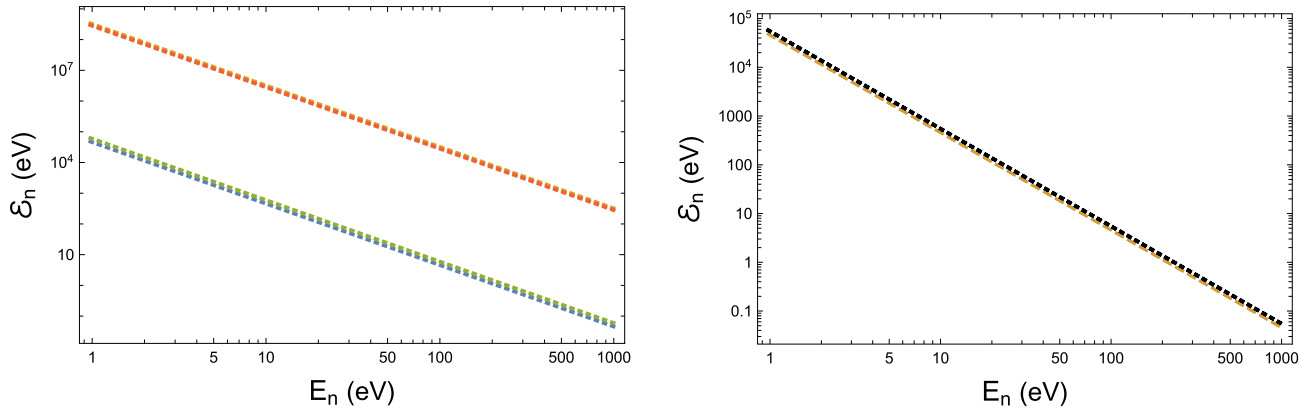

Fig. 17 Left: we plot the deposited energy in a 10^8 coil system by monopolium Rydberg states as a function of binding energy for two velocities .001 and 0.99 for Schwinger scheme (dashed) and for Dirac Scheme (dotted). For these small binding energies, both schemes coincide. We have slightly changed the velocities to 0.0012 and 0.987 in the Dirac scheme to show the two results. Right: The deposited energy in a 10^8 coil system as a function of binding energy for two monopole masses of 1TeV and 10 TeV. For small E_n, the deposited energy in the Schwinger (dashed) and Dirac (dotted) schemes are equal and independent of the monopole mass for equal binding energy

Let us assume that we have one of those monopolia of $r_n \sim 10^{-3}$mm traversing at $v_M \sim 0.001$ a coil system of 40 m long with $N \sim 10^8$ coils made of a good conductor $\varrho \sim 10^{-8}$ Ohm m, with $R \sim 0.01$ mm and $r_s \sim 0.0001$ mm. In Fig. 17, we show the energy deposited in the coil system. For high Rydberg states close to the dissociation limit, the deposited energy is large, independent of monopole mass for equal binding energy, and in the region of interest, both schemes coincide. The difference between the Dirac and Schwinger scheme is in the lifetime as seen in Fig. 16.

As we shall see in detail later, the coil system detector with nanowatt potentiometers is suited to detect single events in the line with the original monopole detectors [15–19].

5.2 Cosmological heavy monopolium

Let us pursue the study of cosmological monopolium either heavy GUT or Kaluza–Klein monopolium. The very high n Rydberg states of monopolium below the dissociation limit in the Earth's magnetic field have large lifetimes. The discussion related to the effect of the induced current on the particle velocity can be easily generalized also to heavy monopolium. The huge mass of the monopolium states leads to small accelerations, and therefore, the effect on the traveling particle velocity is here also negligible.

For GUT monopoles, the Parker bound can be overcome when monopole-antimonopole bind. In this case, by equating the binding energy to the dissociation energy as above but using a mass for the monopole of 10^{16} GeV, we get a limiting value for monopolia of sizes $r_n \lesssim 10^{-3}$ mm which correspond to binding energies $E_n \gtrsim 1$ eV as before. The velocity of the monopolia, in this case, is also the intergalactic gravitational velocity $v_M \sim 10^{-3}$ which is independent of mass. The crucial ingredients of our previous calculation, binding energy and size, remain the same, and the analysis follows previous calculation for the very high Rydberg states leading to results similar to those shown in Fig. 17 for the deposited energy since it does not depend on the monopole mass for fixed binding energy. The decay distance is much larger for heavy monopoles since the ratio $(E_n/m)^3$ entering the spontaneous emission

lifetime, Eq. (49), is much smaller. Despite this difference, the decay distances are so large for both light and GUT monopolia that their chances of detection are very similar and only the determination of their mass would distinguish them.

The idea behind Kaluza–Klein (KK) theories is that the world has more than three spatial dimensions and some of them are curled up to form a circle so small as to be unobservable [11, 12]. KK theories have been the subject of revived interest in recent years since many standard model extensions in extra dimensions yield KK theories. KK theories contain a very rich topological structure, which includes very heavy monopoles whose mass is around the Planck mass [13, 37]. Most importantly, they also contain other soliton solutions in different topological sectors. In particular, the dipole, has the quantum numbers of a monopole-antimonopole bound state. As we have seen above, in conventional gauge theories, monopolium has vacuum quantum numbers and annihilates. However, in KK theories, monopolium does not belong to the topological sector of the vacuum, and therefore, it is classically stable [13]. In realistic scenarios, the dipole does not have vacuum quantum numbers [14, 38–40], and its structure is described in terms of some parameter r (distance between center of the poles), which approaches the monopole-antimonopole structure as r becomes large. The dipole can thus be interpreted as a bound state with a mass smaller than twice the monopole mass. The parameter r describes the magnetic moment of the dipole. The ground state (smallest mass) dipole, i.e., when $r \to 0$, has vanishingly small dipole moment, and therefore, it is electromagnetically neutral and thus has gravitational interaction only. When $r > 0$, we can ascribe these states to excited states of monopolium, and in the large r limit, we are discussing the equivalent of Rydberg states. Since those states are very much like an elongated monopole-antimonopole structure separated by a distance r, the magnetic moment is

$$\mathcal{M}_r \sim g\, r. \tag{57}$$

Once this similarity is exploited, again the parameters that play a role in the calculation are the monopole mass $m \sim M_{\text{Plack}} \sim \sqrt{\frac{\hbar c}{G}} \sim 10^{19}$ GeV where G is the gravitational constant $1.32\,10^{-39}$ fm/GeV, the binding energy, $E_r = 2M - M_r$, and the mass independent gravitational velocity $v_r \sim 10^{-3}$. In this case, again binding energies and sizes will be determined by avoiding dissociation. Let us use for our calculation the mass formula for the dipole of the Gross–Perry model [13, 14]

$$M_r = 2\left(m - \frac{M_r^2}{\sqrt{4M_r^2 + \frac{r^2}{G^2}}}\right), \tag{58}$$

where $m \sim \frac{M_{\text{Planck}}}{4\sqrt{\alpha}}$ the monopole mass, with $M_{Planck} \sim 1.22\,10^{19}$ GeV, M_r is the monopolia mass and r is given in fm and the masses in GeV. For large r, we obtain the binding energy approximation for the Rydberg states

$$E_r \sim \frac{8Gm^2}{r}. \tag{59}$$

Equating this energy to the dissociation energy $E_r = g B_E r \sim \frac{g B_E r}{0.197\,\text{GeV fm}}$, where B_E is measured in GeV^2 and r in fm, we get the maximum monopolium size in the Earth at $r = \sqrt{\frac{1.58\,\text{GeV fm}\,Gm^2}{g B_E}}$ which turns out to be $r \sim 10^{-2}$ mm with a binding energy is $E_r \sim 1$ eV. Size and binding energy are similar to the ones above. The physics is going to be the same, and therefore, the experimental setup might be also suitable for this monopole dynamics. Only a kinematic detector will distinguish between the three types of monopoles studied. The fact that the KK monopolia are classically stable does not make any difference for detection purposes because the lifetime for all other scenarios is very large for Rydberg states. We foresee in this case two mechanisms of production given their huge mass, either a primordial mechanism which took place before inflation [14] or a cataclysmic collision of monopolium clouds after inflation. The former will produce mostly ground state or low excited monopolia with small values of r, very difficult to detect with the present setup. The latter will produce highly excited states with large r, but very few in number. Again in this scenario, we need detectors which look at extraordinary events, and for monopolium, a coil system might be adequate.

One question which might have arisen to the reader is if these large monopolium might be dissociated when passing through matter. Cosmic monopolium must traverse the atmosphere to reach any terrestrial detector. This question requires a deeper investigation but we give here some qualitative arguments. On the Earth's surface, the distance between molecules is 10^{-6} mm, which means that large monopolia, 10^{-3} mm, interact with many molecules, whose size is order Angstrom $\sim 10^{-7}$ mm, thus they behave point-like for Rydberg monopolia. The simplest model is that the atmosphere seen from a moving monopolium is an unpolarized gas of magnetic dipoles. Two types of interactions are of interest. One is the magnetic charge to magnetic moment interaction $\sim \frac{g\,\vec{m}\cdot\vec{r}}{r^3}$, where $\vec{m}$ is the magnetic moment of the molecule, and $\vec{r}$ is the relative distance between the magnetic charge and the molecule. The other is the interaction of magnetic moments of monopolium $\vec{\mathcal{M}}$ with $\vec{m}$ of the molecule, which is a complex expression but which can be qualitatively approximated by $\frac{\vec{m}\cdot\vec{\mathcal{M}}}{r^3}$. We note that both of them depend on the magnetic moment of the molecules. If we consider the atmosphere as an unpolarized gas of molecules, the two interactions will cancel on the average, and therefore, monopolium will remain bound and continue its motion unperturbed. A more detailed study will be presented elsewhere, but one can argue that for distances charge-molecule or molecule-monopolium of 10^{-7} mm, the binding interaction $\frac{g^2}{r_M}$ is stronger and therefore dissociation does not occur, nor does monopolium slow down by binding itself with many molecules.

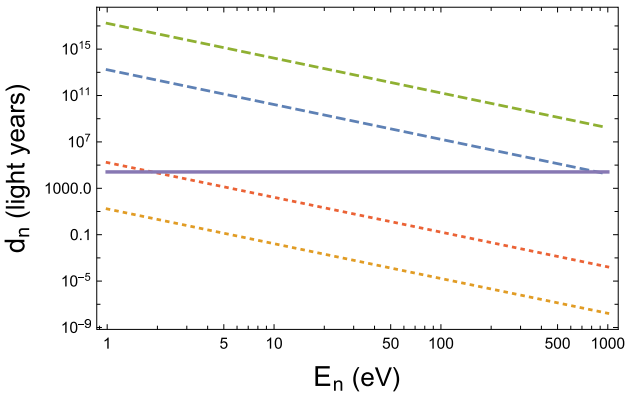

Fig. 18 Distance traveled by a monopolium Rydberg state as a function of binding energy at a velocity of $v_M \sim 0.001$ for Dirac (dotted) and Schwinger (dashed) scheme. The lower curve in each case corresponds to a monopole mass of 1 TeV and the upper curve to a mass of 100 TeV. The solid line gives the distance from the center of the galaxy to the earth $\sim$ 25800 light years

6 Concluding remarks

Monopolium, a bound state of monopole-antimonopole, has no magnetic charge and in its ground state no magnetic moment, being therefore very difficult to detect directly. In conventional gauge theories, it has the quantum numbers of the vacuum and annihilates into photons, and these disintegrations have been intensively studied [10, 26, 28–30, 35]. In Kaluza–Klein theories, monopolium is classically stable and therefore very long lived [13, 14] but its detection problems still persist since it only interacts gravitationally.

What happens with excited monopolium states? This paper deals with the study of the excited states of monopolium. Excited states have permanent magnetic moments, and their interaction with magnetic and electric fields is known. We have used a theoretical analysis of magnetic dipole detection to learn about excited monopolium states. Analyzing the detailed characteristics of excited monopolium states, we have discovered many properties, in particular, for the high n Rydberg states.

The first part of the analysis deals with a theoretical description of the interaction of magnetic moment with coils and solenoids both for conductors and superconductors. Given that the difference between the two is not large and that our aim is to learn about the behavior of Rydberg states more than to perform a detailed experimental analysis of detection, we have continued only with conductors.

Our analysis shows that only very high lying Rydberg states might be detectable with coil systems. Those with a large lifetime, that could escape the beam and be detected, given their small production cross section and the limited luminosity, cannot be produced at colliders [41]. Therefore, we have to resort to cosmic monopolium.

Since bound states do not absorb energy from the galactic magnetic fields, monopolia can overcome the Parker bound. When these excited monopolia reach the Earth, the Earth's magnetic field might break them giving rise to monopole-antimonopole pairs, which might not annihilate since the excited states are very large, $10^{-3} - 10^{-2}$ mm. Typical magnetic monopole detectors can be successful in seeing them [15–19, 42]. However, for larger binding energies, the monopolium Rydberg states remain, and they are ideal candidates for the setup presented here.

Let us look more carefully into the detection of excited monopolium states. In Fig. 18, we plot the distance traveled as a function of binding energy by an excited monopolium for a $v_m \sim 0.001$ and two monopole masses of 1 and 100 TeV. The solid line represents the distance to the center of the galaxy. Thus, Rydberg states produced in the center of the galaxy would reach our detector for masses of 1 TeV or larger in the Schwinger scheme and only for masses of 100 TeV or larger in the Dirac scheme. However, light monopolia could be produced by the collision of two energetic photons anywhere closer to the earth and they could be also detected in the Dirac scheme. Inflationary monopolia are almost stable by our standards, and they could reach the Earth from anywhere.

All the states studied, including inflationary monopolium, have large lifetimes as can be seen from the distance they can travel and therefore will appear mostly stable for detectors of tens of meters long. We use Faraday-Lenz coil systems to signal their presence. One important result we have proven is that for fixed binding energy, the deposited energy is mass independent all the way to the inflationary monopolia, which have binding energies $E_n > 1$ eV. In Fig. 19, we show the energy deposited in the coil system described before formed by coils of radius $R = 0.01$ mm, separated $2r_s = 0.0001$ mm, where r_s is the radius of the section of the coil, and a resistivity $\varrho = 10^{-8}$ Ohm m, of length 40 m and $N = 10^8$ coils. The dashed line corresponds to the Schwinger scheme and the dotted line to the Dirac scheme for a velocity of $v_M \sim 0.001$. The solid lines correspond to the lowest deposited energy a potentiometer with 1 picowatt ($\sim$ 0.8 eV) and 1 nanowatt ($\sim$ 800 eV) precision would measure, assuming that the Rydberg states cross the whole 40 m detector at a speed of $v_M \sim 0.001$. Thus, in both schemes, we are able to detect the passing of the Rydberg states with present day available high resolution potentiometers. The inflationary monopolium Rydberg states would have similar deposited energies.

Finally, a natural property of excited states is the emission of cascading photons. In our case, since the Rydberg states have a very small binding energy, there will be cascading photons of atomic energy $\sim 1-100$ eV, together with other cascading photons associated with the lower states of much higher energy. These photons would be a characteristic feature of excited monopolium in all three scenarios. Thus, a Faraday-Lenz coil system supplemented by photon detectors could describe the passing of monopolia Rydberg

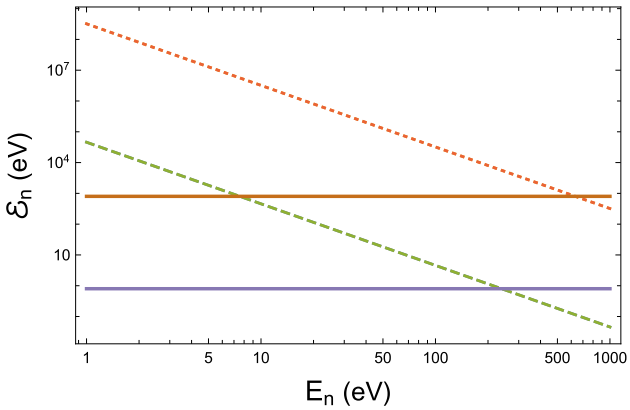

Fig. 19 Deposited energy as a function of binding energy in both Schwinger (dashed) and Dirac (dotted) schemes for a detector of 10^8 coils, and length of 40 m with the properties specified in the text. The solid lines represent the lowest energy that a potentiometer with a 1 picowatt and 1 nanowatt precision would measure during the time the Rydberg states traverses the full detector at a speed $v_M \sim 0.001$

states. In conclusion, we have seen that excited states of monopolium have besides gravitational interaction an electromagnetic interaction associated with their magnetic moments. We have investigated their properties and have arrived to the conclusion that only the very high Rydberg states live long enough and have sufficiently large magnetic moment to be detected in cosmological scenarios.

Acknowledgements Vicente Vento would like to thank Daniel Cano, Fernando Martínez, Vassia Mitsou and José Luis Tain, for useful conversations. HF and CAGC were partially supported by ANPCyT, Argentina. VV was supported in part Ministerio de Ciencia e Innovación and Agencia Estatal de Investigación of Spain MCIN/AEI/10.13039/501100011033, European Regional Development Fund Grant No. PID2019-105439 GB-C21 and by GVA PROMETEO/2021/083.

Funding Open Access funding provided thanks to the CRUE-CSIC agreement with Springer Nature.

Data availability All data generated or analyzed during this study are included in this published article.

References

1. P.A.M. Dirac, Quantised singularities in the electromagnetic field. Proc. R. Soc. Lond. A **133**, 60–72 (1931)
2. P.A.M. Dirac, The Theory of magnetic poles. Phys. Rev. **74**, 817–830 (1948)
3. G. 't Hooft, Magnetic Monopoles in Unified Gauge Theories. Nucl. Phys. B **79**, 276–284 (1974)
4. A.M. Polyakov, Particle spectrum in the quantum field theory. JETP Lett. **20**, 194–195 (1974)
5. H. Georgi, S.L. Glashow, Unified weak and electromagnetic interactions without neutral currents. Phys. Rev. Lett. **28**, 1494 (1972)
6. J. Preskill, Magnetic monopoles. Ann. Rev. Nucl. Part. Sci. **34**, 461–530 (1984)
7. A.K. Drukier, S. Nussinov, Monopole pair creation in energetic collisions: Is it possible? Phys. Rev. Lett. **49**, 102 (1982)
8. Y.B. Zeldovich, M.Y. Khlopov, On the concentration of relic magnetic monopoles in the universe. Phys. Lett. B **79**, 239–241 (1978)
9. V. Vento, Hidden Dirac monopoles. Int. J. Mod. Phys. A **23**, 4023–4037 (2008)
10. L.N. Epele, H. Fanchiotti, C.A.G. Canal, V.A. Mitsou, V. Vento, Looking for magnetic monopoles at LHC with diphoton events. Eur. Phys. J. Plus **127**, 60 (2012)
11. T. Kaluza, Zum unitätsproblem der physik. Int. J. Mod. Phys. D **27**(14), 1870001 (2018)
12. O. Klein, Quantum theory and five-dimensional theory of relativity (in German and English). Z. Phys. **37**, 895–906 (1926)
13. D.J. Gross, M.J. Perry, Magnetic monopoles in Kaluza–Klein theories. Nucl. Phys. B **226**, 29–48 (1983)
14. V. Vento, Primordial monopolium as dark matter. Eur. Phys. J. C **81**(3), 229 (2021)
15. B. Cabrera, First results from a superconductive detector for moving magnetic monopoles. Phys. Rev. Lett. **48**, 1378–1380 (1982)
16. K.A. Milton, Theoretical and experimental status of magnetic monopoles. Rept. Prog. Phys. **69**, 1637–1712 (2006)
17. B. Acharya et al., The physics programme of the MoEDAL experiment at the LHC. Int. J. Mod. Phys. A **29**, 1430050 (2014)
18. B. Acharya et al., The physics programme of the MoEDAL experiment at the LHC. Int. J. Mod. Phys. A **29**, 1430050 (2014)
19. L. Patrizii, M. Spurio, Status of searches for magnetic monopoles. Ann. Rev. Nucl. Part. Sci. **65**, 279–302 (2015)
20. V. Vento, M. Traini, Scattering of charged particles off monopole-anti-monopole pairs. Eur. Phys. J. C **80**(1), 62 (2020)
21. A. Apyan, A.B. Apyan, M. Schmitt, Detecting neutrino magnetic moments with conducting loops. Phys. Rev. D **77**, 037901 (2008)
22. H. Hirakawa, A. Futakawa, Inductance of superconducting solenoids. Cryogenics **13**(5), 287–289 (1973)
23. N.E. Mavromatos, V.A. Mitsou, Magnetic monopoles revisited: Models and searches at colliders and in the Cosmos. Int. J. Mod. Phys. A **35**(23), 2030012 (2020)
24. C. Goebel, Quanta, in *Essays in Theoretical Physics*. ed. by P.G.O. Freund, C.J. Goebel, Y. Nambu (University of Chicago Press, Chicago, 1970)

25. L.I. Schiff, Quarks and magnetic poles. Phys. Rev. **160**, 1257–1262 (1967)
26. N.D. Barrie, A. Sugamoto, K. Yamashita, Construction of a model of monopolium and its search via multiphoton channels at LHC. PTEP **2016**(11), 113B02 (2016)
27. S. Baines, N.E. Mavromatos, V.A. Mitsou, J.L. Pinfold, A. Santra, Monopole production via photon fusion and Drell-Yan processes: MadGraph implementation and perturbativity via velocity-dependent coupling and magnetic moment as novel features. Eur. Phys. J. C **78**(11), 966 (2018). (**Erratum: Eur.Phys.J.C 79, 166 (2019)**)
28. N.D. Barrie, A. Sugamoto, M. Talia, K. Yamashita, Searching for monopoles via monopolium multiphoton decays. Nucl. Phys. B **972**, 115564 (2021)
29. L.N. Epele, H. Fanchiotti, C.A. Garcia Canal, V. Vento, Monopolium: the key to monopoles. Eur. Phys. J. C **56**, 87–95 (2008)
30. L.N. Epele, H. Fanchiotti, C.A.G. Canal, V. Vento, Monopolium production from photon fusion at the Large Hadron Collider. Eur. Phys. J. C **62**, 587–592 (2009)
31. P.A.M. Dirac, On the annihilation of electrons and protons. Proc. Camb. Philos. Soc. **26**, 361–375 (1930)
32. A. Ore, J.L. Powell, Three photon annihilation of an electron–positron pair. Phys. Rev. **75**, 1696–1699 (1949)
33. D.A. Dicus, V.L. Teplitz, Circumvention of Parker's bound on galactic magnetic monopoles. Nature **303**, 408–409 (1983)
34. J.S. Schwinger, K.A. Milton, W.-Y. Tsai, L.L. DeRaad Jr., D.C. Clark, Nonrelativistic Dyon–Dyon scattering. Ann. Phys. **101**, 451 (1976)
35. H. Fanchiotti, C.A. García Canal, V. Vento, Multiphoton annihilation of monopolium. Int. J. Mod. Phys. A **32**(35), 1750202 (2017)
36. M.S. Turner, E.N. Parker, T.J. Bogdan, Magnetic monopoles and the survival of galactic magnetic fields. Phys. Rev. D **26**, 1296 (1982)
37. R.D. Sorkin, Kaluza-Klein monopole. Phys. Rev. Lett. **51**, 87–90 (1983)
38. E. Newman, L. Tamburino, T. Unti, Empty space generalization of the Schwarzschild metric. J. Math. Phys. **4**, 915 (1963)
39. S.W. Hawking, Gravitational instantons. Phys. Lett. A **60**, 81 (1977)
40. G.W. Gibbons, S.W. Hawking, Classification of gravitational instanton symmetries. Commun. Math. Phys. **66**, 291–310 (1979)
41. H. Fanchiotti, C.A.G. Canal, M. Traini, V. Vento, Looking for monopolium excited states with electromagnetic detectors. arXiv:2110.02646 [hep-ph]
42. V.A. Mitsou, MoEDAL physics results and future plans. PoS **CORFU2019**, 009 (2020)